

Energy transfer from tunneling electrons to excitons

Sotirios Papadopoulos,^{1,*} Lujun Wang,^{1,*} Takashi Taniguchi,² Kenji Watanabe,³ and Lukas Novotny^{1,†}

¹*Photonics Laboratory, ETH Zurich, 8093 Zurich, Switzerland.*

²*International Center for Materials Nanoarchitectonics,*

National Institute for Materials Science, 1-1 Namiki, Tsukuba 305-0044, Japan

³*Research Center for Functional Materials, National Institute for Materials Science, 1-1 Namiki, Tsukuba 305-0044, Japan*

Excitons in optoelectronic devices have been generated through optical excitation, external carrier injection, or employing pre-existing charges. Here, we reveal a new way to electrically generate excitons in transition metal dichalcogenides (TMDs). The TMD is placed on top of a gold-hBN-graphene tunnel junction, outside of the tunneling pathway. This electrically driven device features a photoemission spectrum with a distinct peak at the exciton energy of the TMD. We interpret this observation as exciton generation by energy transfer from tunneling electrons, which is further supported by a theoretical model based on inelastic electron tunneling. Our findings introduce a new paradigm for exciton creation in van der Waals heterostructures and provide inspiration for a new class of optoelectronic devices in which the optically active material is separated from the electrical pathway.

Exciton generation in TMDs

Transition metal dichalcogenides (TMDs) have attracted attention due to their interesting electronic and optical properties. In monolayer form, they exhibit a direct bandgap [1], responsible for radiative electron-hole recombination [2]. TMDs support excitons with high binding energies due to quantum confinement [3], making their optical properties to be dominantly defined by their excitonic states [4–6]. Exciton generation in TMDs was first studied through optical excitation [1, 2, 7–10]. Later, combination with conductors (i.e. graphene) and insulators (i.e. hexagonal boron nitride) [11, 12] allowed the design and fabrication of light-emitting van der Waals (vdW) heterostructures with TMDs as the optically active material [13–28]. In these studies, excitons are electrically generated through direct charge injection [13–27] or through charge impact at high alternating voltages [28]. Here, we introduce a different way to generate excitons in TMD based tunneling devices. We use the rich platform of 2D materials to demonstrate excitonic light emission from tunnel junctions where the TMD is located outside of the current pathway.

The studied device structure is illustrated in Fig. 1A. The TMD and the tunnel junction are electrically decoupled, preventing exciton generation through direct electron-hole injection. The emission spectrum of such a device features a distinctive peak at the exciton energy, as shown in Fig. 1B. We attribute the generation of excitons to energy transfer (ET) from tunneling electrons. ET from a donor to an acceptor is mediated by dipole-dipole coupling [29, 30]. It is an electromagnetic effect that is dominant at the near-field region of an emitter and has been extensively studied in biological systems [31], molecular assemblies [32], solid-state quantum dots [33] and photosynthetic membranes [34]. It has been also used for color conversion and broadband source design as an energy exchange channel between different fluorophores [35, 36]. Recent STM studies discuss the possibility of ET in tunneling systems [26, 27] without however providing any conclusive observation. Here we make use of atomically thin

2D materials and the flat interfaces between them to preserve optical coupling in near-field distances between a TMD and a tunnel junction. Our results reveal the role of ET between electrons and excitons in tunneling-based light emitting devices.

TMD-coupled tunnel junctions

Our devices are fabricated by stacking mechanically exfoliated flakes of 2D materials with a dry pickup and transfer technique (see supplementary materials for details). The resulting tunnel junctions consist of a graphene and a gold electrode separated by a hexagonal boron nitride layer (hBN) of 2.3 nm thickness acting as a tunneling barrier. The TMD is stacked on top of the junction and optionally separated from the graphene electrode by a second hBN layer.

Figure 2A shows a false-color microscope image of the device with an outline of the different flakes. The device area is indicated by a white dashed box. The tunnel junction area is defined by the overlap of the gold electrode and the graphene flake. The WSe₂ flake is only partially covering the tunneling area. This creates two different tunneling regions, with and without WSe₂ on top. We electrically and optically characterize the device by applying a bias voltage (V_b) between the gold and graphene electrodes, as indicated in Fig. 2A, and we collect the emitted light with a high-numerical aperture objective (see supplementary materials). The current and conductance measurements suggest that tunneling occurs between graphene and gold (see Fig. S1A). The spectra emitted from the whole tunneling area for various V_b values are presented in Fig. 2B. There are two distinct contributions in the spectra. A broad emission at lower energies and a narrow emission peak at 1.63 eV (762 nm). The broad emission shifts to higher photon energies as V_b is increased. This behavior suggests that the emission originates from inelastic electron tunneling that couples to radiative modes of the free-space continuum (*photon-coupling*) with eV_b being the cut-off energy of emission [37, 38]. The narrow peak at 1.63 eV cor-

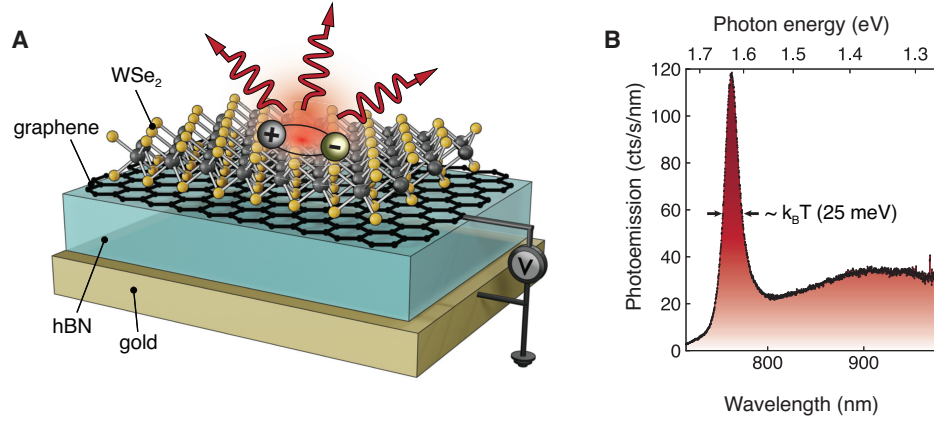


FIG. 1. **Exciton generation in TMD-coupled tunnel junctions.** (a) Device composed of a WSe₂-coupled graphene-hexagonal boron nitride (hBN)-gold tunnel junction. The WSe₂ layer is stacked on top of the junction. When a bias voltage V_b is applied between graphene and gold, excitons are generated in WSe₂. (b) Measured spectrum at room temperature of the electrically generated emission for $V_b = 2$ V. The peak position matches the WSe₂ exciton energy and the spectral width matches the thermal energy $k_B T$.

responds to the neutral 1s exciton of WSe₂ and its narrow width of around 25 meV can be attributed to graphene filtering [39]. It has been shown that charge transfer between graphene and TMDs, filters the TMD photoluminescence spectra from any charged exciton contributions [39]. To further our understanding, we study the emission distribution for different spectral regions. Real space images of the photoemission are presented in Fig. 2C, where we observe that the area covered by WSe₂ dominates the emission and in Fig. 2D, where the emission is filtered by a band-pass filter at 900 nm. This is a spectral region where the excitonic contribution is much reduced and the emission extends over both device areas. This indicates that the broad low energy contribution indeed originates from *photon-coupling* and is not associated with the presence of WSe₂. To understand the angular emission of the device we record Fourier-space images. Fig. 2E shows the Fourier space image of the full emission spectrum whereas Fig. 2F depicts the Fourier space image of the bandpass filtered light around 900 nm. For the spectrally filtered measurement at 900 nm, the emission vanishes at the center of the Fourier space ($k_x = k_y = 0$) (Fig. 2F) indicative for an out-of-plane dipole orientation. This is characteristic of inelastic electron tunneling where the transition dipole is oriented along the electron path. On the other hand, when measuring the full spectrum, the Fourier space image (Fig. 2E) is not zero at $k_x = k_y = 0$, which indicates an in-plane contribution. This extra contribution is associated with the excitonic emission of WSe₂, which is known to originate from in-plane transitions [40]. We emphasize that in our devices any exciton generation due to electron-hole injection is avoided due to the WSe₂ being outside of the tunneling pathway. This is further supported by the fact that very similar emission spectra are observed for negative V_b (see Fig. S2). For these reasons we conclude that excitons are generated in the TMD by ET from tunneling electrons.

We continue to investigate this exciton generation process

by considering the band-structure diagram shown in Fig. 3A. Upon application of V_b , electrons tunnel from one electrode to the other, elastically or inelastically. In the latter case, the transition dipole associated with the energy loss ΔE couples to available optical modes of the environment. Some of these modes are radiative (photons) as in the case of the broad emission observed in Fig. 2A, or non-radiative, as in the case of ET. This ET mechanism generates excitons in WSe₂ and their spontaneous decay contributes to the narrow emission peak in the spectra of Fig. 2B. Thus, the excitonic emission observed in our device is a two step process, in which the transition energy is first transferred to the WSe₂ exciton and then spontaneously emitted (*exciton-coupling*).

Next, we compare the ET efficiency to the *photon-coupling* efficiency. To do that we first break down the processes to the involved interactions (see pictorial representation in Fig. 3B) and we assign conversion efficiencies. Both *photon-* and *exciton-coupling* processes describe an electron-to-photon ($e\text{-}\gamma$) conversion. *Photon-coupling* is a first order process for which we define an $e\text{-}\gamma$ conversion efficiency as $\eta_{e\text{-}\gamma}$. *Exciton-coupling* is a second order process in which we can assign a combined efficiency $\eta'_{e\text{-}\gamma} = \eta_{e\text{-}x} \cdot \eta_{x\text{-}\gamma}$, where $\eta_{e\text{-}x}$ is the ET efficiency and $\eta_{x\text{-}\gamma}$ is the exciton to photon conversion efficiency. From the spectra shown in Fig. 2B, we can infer a value of 4.3 for the ratio between the photon-coupled emission and the exciton-coupled emission. By taking into account the values for WSe₂ PL efficiency and the graphene quenching (see supplementary materials) we arrive at an estimation of the ratio $\frac{\eta_{e\text{-}x}}{\eta_{e\text{-}\gamma}} \cong 10^4$. This result indicates that ET is orders of magnitude more efficient than direct photon emission. In order to shed light on this surprising finding we analyze in the next section the density of optical states near a monolayer TMD.

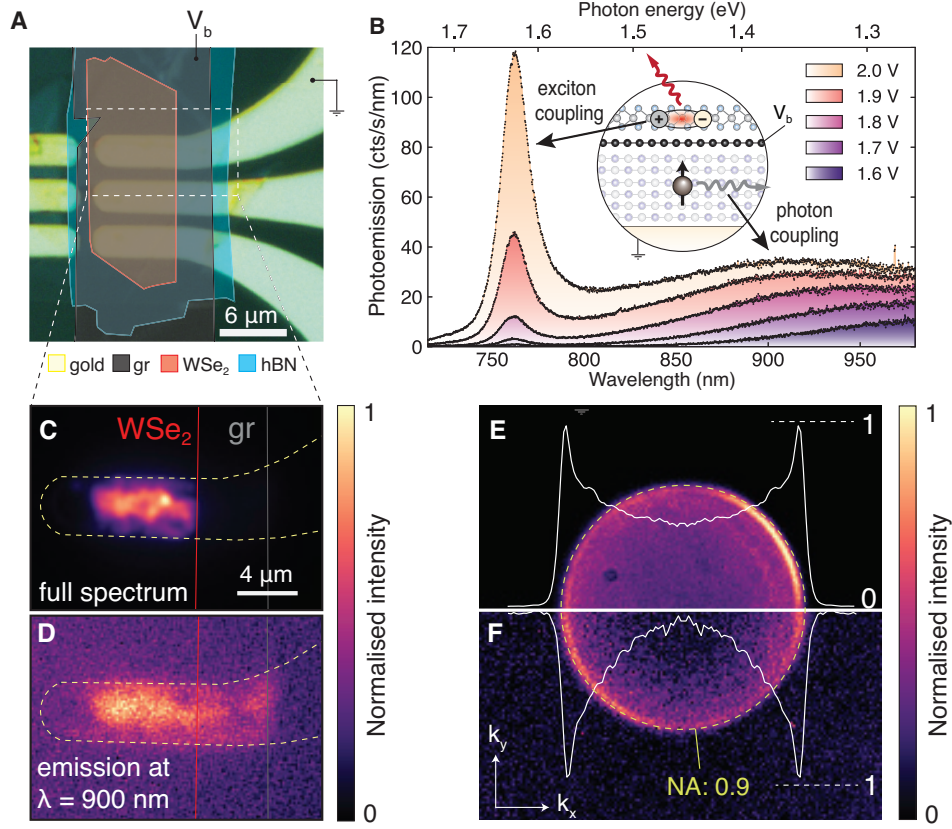


FIG. 2. **WSe₂-coupled tunnel junction.** (a) Optical microscope image in false-color of a fabricated WSe₂-Graphene-hBN-gold device. The different flakes are outlined. The encapsulating hBN flake is not shown for clarity. The dashed frame indicates the device area depicted in (c) and (d). (b) Recorded emission spectra from the whole device area. Contributions from radiative mode coupling (*photon-coupling*) and non-radiative mode coupling (*exciton-coupling*) are observed. Real space (c,d) and Fourier space (e,f) images of the emission from the dashed box in (a) for $V_b = 2$ V. The full emission spectrum is used in (c) and (e) whereas a bandpass filter with center wavelength 900 nm and 40 nm FWHM is used in (d) and (f). Only half of every Fourier space is imaged for ease of comparison. The white solid lines are the rotational averages of the two Fourier spaces in (e) and (f).

Optical density of states near monolayer TMDs

When a dipole interacts with an absorbing material at a distance much smaller than the wavelength, the largest fraction of the dissipated power is associated with non-radiative energy transfer (ET) from the dipole to the material [41, 42]. The rate of this process is related to the local density of optical states (LDOS) ρ_{opt} . In Fig. 3C we show the calculated angular spectral density of the LDOS, $\frac{d\rho_{\text{opt}}}{dk_{\parallel}}$, as a function of k_{\parallel} for the simple case of a dipole at 2 nm distance from a TMD monolayer. Here, k_{\parallel} is the wavevector component along the plane of the TMD monolayer (see inset in Fig. 3C) and k_0 is the wavenumber for a photon energy equal to the exciton energy of WSe₂. The calculated ρ_{opt} for $k_{\parallel} < k_0$ includes radiative modes associated with photon emission (ρ_r) whereas the region $k_{\parallel} > k_0$ accounts for non-radiative modes (ρ_{nr}) associated with ET. ρ_{nr} is orders of magnitude higher than ρ_r . Moreover, the influence of the TMD on ρ_r enhancement is negligible. Hence, the TMD introduces mainly ad-

ditional non-radiative decay channels that are associated with near-field ET ($\rho_{\text{opt}} \cong \rho_{\text{nr}}$), and is the reason for the high $\frac{\eta_{e-x}}{\eta_{e-\gamma}}$ ratio. The ET process in our measurements is highly efficient and shows that near-field interactions at nanoscale distances are dominating the LDOS. Here, we probe this non-radiative interaction by using a direct-gap semiconductor whose luminescence is a direct measure for the ET efficiency. In essence, the TMD acts as a receiving optical antenna that enhances the LDOS and converts non-radiative modes to a measurable signal. We refer to this process as electron-photo-luminescence (ePL) since it is triggered by an electron that transfers energy through optical modes to WSe₂.

Dependence on TMD-Graphene separation

To further test our interpretation, we study the dependence of the excitonic emission on the distance between the TMD and the tunnel junction. A device schematic is shown in Fig. 4A where we vary the coupling to the TMD by chang-

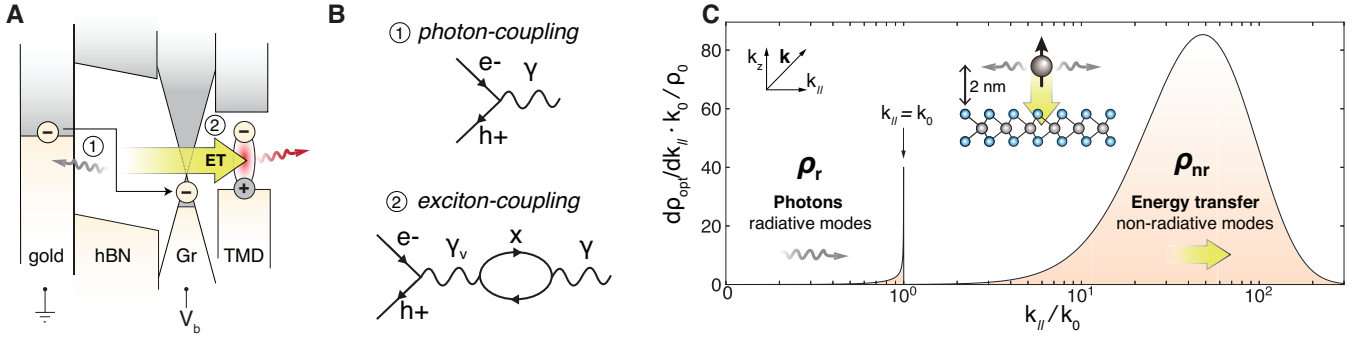


FIG. 3. **Photon and exciton coupling of inelastic tunneling electrons.** (a) Band diagram of the TMD-coupled tunnel junction. A voltage V_b is applied across the hBN barrier between graphene and gold electrodes. Part of the electrons tunnel inelastically. They either couple to radiative modes (1) or couple non-radiatively to the TMD via ET (2). The generated excitons decay radiatively making the ET process detectable in the farfield. (b) Pictorial representation of the physical processes involved in the light emission. In (1) electron-hole recombination is followed by photon emission. In (2) ET is depicted as a virtual photon γ_v that couples to the TMD and creates an electron-hole pair (x). (c) Angular spectral density of ρ_{opt} for the case of an out-of-plane dipole placed 2 nm away from a monolayer WSe₂. Optical properties are taken from [4]. The contribution of non-radiative modes (ρ_{nr}) is substantially higher than the contribution of radiative modes (ρ_r). The calculation assumes a photon energy of 1.68 eV, matching the exciton energy of [4]. The x-axis is normalized by the vacuum wavenumber k_0 and the y-axis is normalized by ρ_0/k_0 , where ρ_0 is the vacuum LDOS. Inset in (c) illustrates the calculated system.

ing the thickness d_s of a hBN spacer layer (s-hBN) in different device regions. Figure 4B shows the emitted light from a device where the s-hBN presents steps in thickness in the tunnel junction area. Four regions of emission are created. Three with different s-hBN thicknesses (6, 5 and 4 layers) and one without WSe₂ on top. We observe that the emission gets stronger the thinner the s-hBN is. As evidenced by the spectra shown in Fig. 4C the enhanced emission can be entirely attributed to the strength of the excitonic peak. We thus find that the excitonic contribution increases for thinner s-hBN in contrast to the broadband background that doesn't show any major change. A comparison of the excitonic emission intensity I_x for different d_s at $V_b = 2$ V is given in Fig. 4D. To compare different devices we normalize I_x by the area of emission, the PL efficiency and the background level (see supplementary materials). The data points in Fig. 4D clearly show that the rate of exciton generation, and hence the ET rate, decay superlinearly with the separation d_s .

I_x can be modeled by calculating the exciton generation rate Γ_x . By using inelastic tunneling theory [43] Γ_x assumes the following expression:

$$\Gamma_x(V_b, d_s) \propto \int_0^\infty \eta_{\text{abs}}(\omega) \frac{\gamma_{\text{inel}}^0(\omega, V_b)}{\rho_0(\omega)} [\rho_{\text{opt}}(\omega, d_s) - \rho_{\text{opt}}(\omega, \infty)] d\omega \quad (1)$$

where ω is the angular frequency, η_{abs} is the absorption spectrum of monolayer WSe₂ [7], γ_{inel}^0 is the inelastic tunneling spectral rate in vacuum and ρ_0 is the vacuum LDOS. We approximate the LDOS responsible for exciton generation by $\rho_{\text{opt}}(\omega, d_s) - \rho_{\text{opt}}(\omega, \infty)$ which assumes that the states provided by the TMD, leading to exciton generation, vanish for $d_s \rightarrow \infty$. See supplementary materials for more information on the calculation. The calculated Γ_x as a function of distance

d_s and for $V_b = 2$ V is plotted in Fig. 4D. It agrees well with the distance dependent measurement. Interestingly, both Γ_x and the measured data can be described by a simple inverse square law, as shown in Fig. 4D. Similar observations were reported for ET between optically excited TMDs [44]. The good agreement between our theoretical model and our experimental measurements supports our interpretation.

Monolayer vs bilayer TMD

We continue our study by using a different TMD (MoSe₂) and by comparing ET for monolayers (1L) and bilayers (2L). Figure 5A shows a schematic of the device and the measured ePL spectra. The emission for 2L MoSe₂ (I_{2L}^{ePL}) is less intense than for 1L MoSe₂ (I_{1L}^{ePL}) owing to the indirect bandgap of 2L MoSe₂. To compare this ET-mediated photoluminescence (ePL) with optically excited photoluminescence (PL) we optically excite the two regions with a laser and measure the corresponding emission spectra I_{1L}^{PL} and I_{2L}^{PL} , respectively. The measurements are presented in Fig. 5B. The center wavelengths and the shapes of PL and ePL spectra match very well, which supports the interpretation that ePL corresponds to spontaneous exciton emission. We note however, that the ratios $I_{1L}^{\text{PL}}/I_{2L}^{\text{PL}}$ and $I_{1L}^{\text{ePL}}/I_{2L}^{\text{ePL}}$ are different. Interestingly, the $I_{1L}^{\text{PL}}/I_{2L}^{\text{ePL}}$ ratio depends on V_b . In fact, I_{2L}^{ePL} is stronger than I_{1L}^{PL} for low voltages and a crossing occurs near $V_b = 1.75$ V, as shown in Fig. 5C, which depicts the integrated spectra for different voltages. By employing the model in Eq. 1 we are able to reproduce this effect. The result of this calculation is given in the inset of Fig. 5C. The reason for this voltage dependence are the different optical properties of 1L and 2L MoSe₂, i.e. the absorption spectrum η_{abs} of 2L MoSe₂, which features a cut-off energy at lower energies and stronger ab-

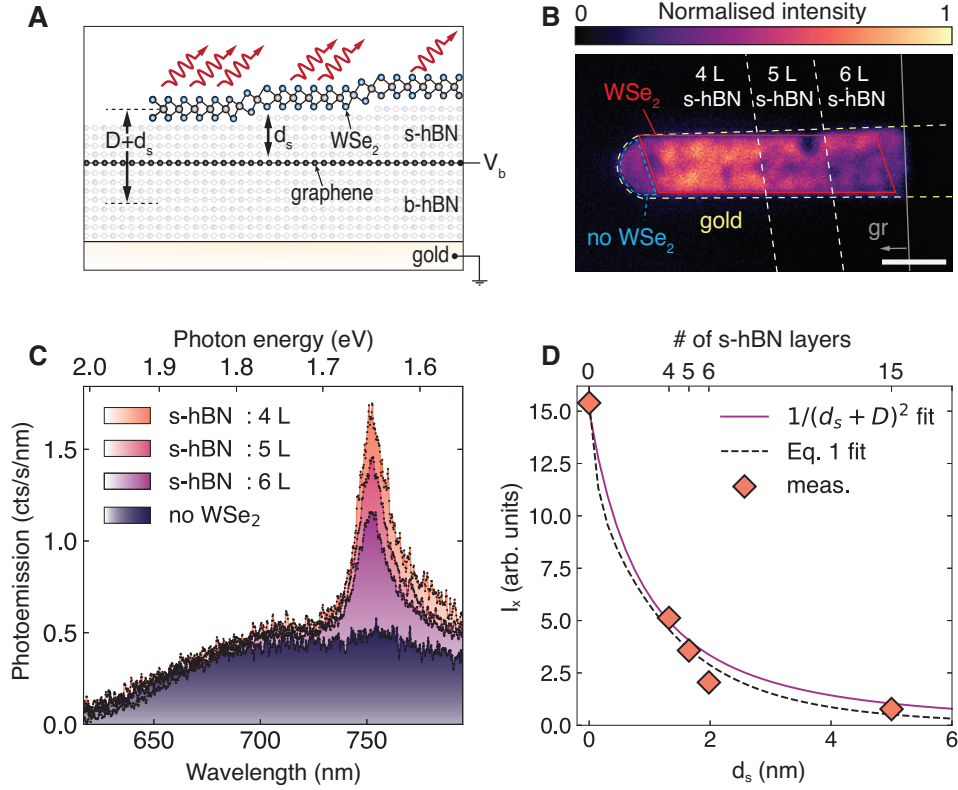


FIG. 4. Distance dependent energy transfer. (a) Schematic of a TMD separated from the tunnel junction by a spacer-hBN (s-hBN). The coupling strength between TMD and the tunnel junction is varied using different s-hBN thicknesses d_s . (b) Real-space image of emission from the WSe₂/s-hBN/Gr/b-hBN/gold device. Strongest emission is observed from the thinnest s-hBN region. The emission is filtered with a bandpass filter ($\lambda_{center} = 750$ nm and fwhm = 40 nm). The scale bar is 4 μ m. (c) Spectra measured on areas with different s-hBN thickness and for $V_b = 2$ V. The broad spectral background corresponds to direct photon coupling and is also observed in areas with no WSe₂. (d) Excitonic emission I_x as a function of d_s . The values are normalized with the PL efficiency, the emission area and the intensity of background emission. The measurement point at $d_s = 0$ nm refers to the device presented in Fig. 2. The three points between $d_s = 1$ nm and 2.5 nm refer to the device presented in Fig. 4B and the point at $d_s = 5$ nm refers to a third device, for which spectra are presented in Fig. S2. The dashed curve is the result of Eq. 1 and the solid curve is a fit with an inverse square distance function. $D + d_s$ is the distance between the TMD and the center of the b-hBN layer as illustrated in (a).

sorption than the 1L MoSe₂. This explains the earlier onset-voltage for I_{2L}^{ePL} in Fig. 5C. Moreover, the two curves are also affected by the dependence of the LDOS on flake thickness. In fact, our model predicts that the rate of ET to a 2L TMD is lower compared to a 1L despite the fact that the 2L TMD is thicker. This surprising behavior has been studied in the past in optically excited systems [45].

Discussion

The exciton generation mechanism, discussed in this work, is an electromagnetic phenomenon that is usually neglected in the analysis of tunneling driven systems. The tunneling probability of an electron relies on the available electronic states but also optical states. In semiconducting materials, exciton resonances provide non-radiative optical states that couple strongly with inelastic electrons increasing the tunneling probability. This leads to near-field generation of exci-

tons even for applied voltages below the electronic bandgap of the material, thus contributing to sub-bandgap emission. Such low voltage emission has been previously studied with interpretations varying from direct exciton formation [16] to Auger scattering [24]. Here we show that ET from tunneling electrons can contribute to this sub-bandgap emission.

Conclusions

We investigated ET from a tunnel junction to TMD excitons. Our studies are based on vdW tunnel devices in which the TMD is placed outside the electronic pathway, ensuring that there is no direct charge injection into the TMD. We studied photoemission spectra as well as real space and Fourier space emission patterns and we concluded that excitons are generated when the tunnel junction is under bias. This surprising observation is understood by ET from tunneling electrons to excitons. Emission from excitons is observed even

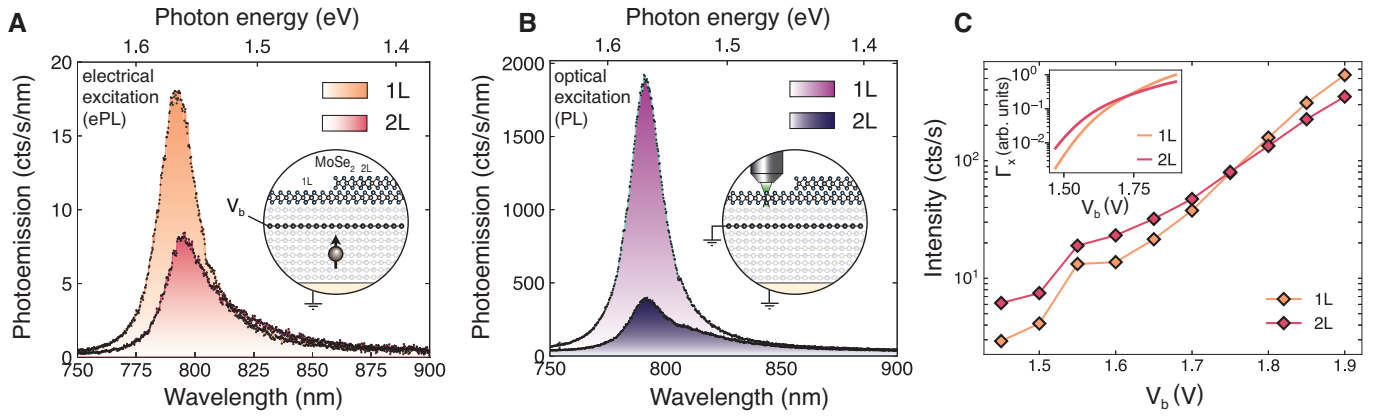


FIG. 5. **Tunnel junctions coupled to monolayer and bilayer MoSe₂.** (a) ePL emission spectra from a device with monolayer (1L) and bilayer (2L) MoSe₂. Spectra taken at $V_b = 1.9$ V. The inset shows the device schematic. (b) PL emission from 1L and 2L regions of the same device. (c) Integrated intensities of the ePL spectra in (a) as a function of V_b . The inset shows corresponding theoretical curves based on Eq. 1.

when the TMD is separated from the junction by a hBN spacer layer. Our calculations reveal that non-radiative modes of the LDOS are strongly increased at the exciton energy. These non-radiative modes are responsible for the efficient energy transfer from the tunnel junction to the TMD. Our theoretical model based on inelastic tunneling theory and near-field coupling is in agreement with our experimental measurements.

The electrical generation of excitons via ET provides new perspectives for the development of optical sources, detectors and sensors. For example, it can be employed for truly chip-scale light sources with applications in electrical pumping scheme for vdW heterostructure lasers [46, 47] or optical sensing schemes [48] that do not rely on external laser sources.

ACKNOWLEDGMENTS

The authors would like to thank Mathieu Luisier, Achint Jain, Martin Frimmer, Ronja Khelifa, Anna Kuzmina, Shengyu Shan and Massimiliano Rossi for fruitful discussions. This study was supported by funding from ETH Zurich under ETH Grant No. ETH-15 19-1 SYNEMA, the ETH Zurich Foundation project number 2013-08 (11) with a donation from the Stavros Niarchos Foundation, and the Swiss National Science Fund under grant number 200020_192362. K.W. and T.T. acknowledge support from the JSPS KAKENHI (Grant Numbers 19H05790, 20H00354 and 21H05233).

AUTHOR CONTRIBUTIONS

S.P., L.W. and L.N. conceived the experiment. S.P. fabricated the devices, performed the measurements, analysed the data, developed the theoretical model and performed the calculations. L.W. supported in the device fabrication. L.W. and

L.N. helped with the data interpretation. K.W. and T.T. provided the high-quality hBN crystals, L.N. initiated and supervised the project. S.P. wrote the paper and all authors discussed the results and worked on the manuscript.

* These two authors contributed equally

† inovotny@ethz.ch

- [1] K. F. Mak, C. Lee, J. Hone, J. Shan, and T. F. Heinz, Atomically thin MoS₂: A new direct-gap semiconductor, *Physical Review Letters* **105**, 2 (2010), 1004.0546.
- [2] A. Splendiani, L. Sun, Y. Zhang, T. Li, J. Kim, C. Y. Chim, G. Galli, and F. Wang, Emerging photoluminescence in monolayer MoS₂, *Nano Letters* **10**, 1271 (2010).
- [3] A. Chernikov, T. C. Berkelbach, H. M. Hill, A. Rigosi, Y. Li, O. B. Aslan, D. R. Reichman, M. S. Hybertsen, and T. F. Heinz, Exciton binding energy and nonhydrogenic Rydberg series in monolayer WS₂, *Physical Review Letters* **113**, 10.1103/PhysRevLett.113.076802 (2014), 1403.4270.
- [4] G. H. Jung, S. J. Yoo, and Q. H. Park, Measuring the optical permittivity of two-dimensional materials without a priori knowledge of electronic transitions, *Nanophotonics* **8**, 263 (2018).
- [5] C. Hsu, R. Frisenda, R. Schmidt, A. Arora, S. M. de Vasconcellos, R. Bratschitsch, H. S. van der Zant, and A. Castellanos-Gomez, Thickness-Dependent Refractive Index of 1L, 2L, and 3L MoS₂, MoSe₂, WS₂, and WSe₂, *Advanced Optical Materials* **7**, 10.1002/adom.201900239 (2019).
- [6] G. A. Ermolaev, Y. V. Stebunov, A. A. Vyshnevyy, D. E. Tatarkin, D. I. Yakubovsky, S. M. Novikov, D. G. Baranov, T. Shegai, A. Y. Nikitin, A. V. Arsenin, and V. S. Volkov, Broad-band optical properties of monolayer and bulk MoS₂, *npj 2D Materials and Applications* **4**, 1 (2020).
- [7] D. Kozawa, R. Kumar, A. Carvalho, K. Kumar Amara, W. Zhao, S. Wang, M. Toh, R. M. Ribeiro, A. H. Castro Neto, K. Matsuda, and G. Eda, Photocurrent relaxation pathway in two-dimensional semiconducting transition metal dichalcogenides, *Nature Communications* **5**, 1 (2014).
- [8] D. H. Lien, S. Z. Uddin, M. Yeh, M. Amani, H. Kim, J. W. Ager, E. Yablonovitch, and A. Javey, Electrical suppression of all nonradiative recombination pathways in monolayer semi-

- conductors, *Science* **364**, 468 (2019).
- [9] M. Amani, D. H. Lien, D. Kiriya, J. Xiao, A. Azcatl, J. Noh, S. R. Madhupathy, R. Addou, K. C. Santosh, M. Dubey, K. Cho, R. M. Wallace, S. C. Lee, J. H. He, J. W. Ager, X. Zhang, E. Yablonovitch, and A. Javey, Near-unity photoluminescence quantum yield in MoS₂, *Science* **350**, 1065 (2015).
 - [10] H. Kim, S. Z. Uddin, N. Higashitarumizu, E. Rabani, and A. Javey, Inhibited nonradiative decay at all exciton densities in monolayer semiconductors, *Science* **373**, 448 (2021).
 - [11] K. S. Novoselov, D. Jiang, F. Schedin, T. J. Booth, V. V. Khotkevich, S. V. Morozov, and A. K. Geim, Two-dimensional atomic crystals, *Proceedings of the National Academy of Sciences of the United States of America* **102**, 10451 (2005).
 - [12] A. K. Geim and I. V. Grigorieva, Van der Waals heterostructures, *Nature* **499**, 419 (2013), 1307.6718.
 - [13] F. Withers, O. Del Pozo-Zamudio, A. Mishchenko, A. P. Rooney, A. Gholinia, K. Watanabe, T. Taniguchi, S. J. Haigh, A. K. Geim, A. I. Tartakovskii, and K. S. Novoselov, Light-emitting diodes by band-structure engineering in van der Waals heterostructures, *Nature Materials* **14**, 301 (2015).
 - [14] M. Paur, A. J. Molina-Mendoza, R. Bratschitsch, K. Watanabe, T. Taniguchi, and T. Mueller, Electroluminescence from multi-particle exciton complexes in transition metal dichalcogenide semiconductors, *Nature Communications* **10**, 1 (2019).
 - [15] R. J. Peña Román, Y. Aua, L. Grasso, F. Alvarez, I. D. Barcelos, and L. F. Zagonel, Tunneling-current-induced local excitonic luminescence in p-doped WSe₂ monolayers, *Nanoscale* **12**, 13460 (2020).
 - [16] J. Binder, F. Withers, M. R. Molas, C. Faugeras, K. Nogajewski, K. Watanabe, T. Taniguchi, A. Kozikov, A. K. Geim, K. S. Novoselov, and M. Potemski, Sub-bandgap Voltage Electroluminescence and Magneto-oscillations in a WSe₂ Light-Emitting van der Waals Heterostructure, *Nano Letters* **17**, 1425 (2017).
 - [17] C. Palacios-Berraquero, M. Barbone, D. M. Kara, X. Chen, I. Goykhman, D. Yoon, A. K. Ott, J. Beitner, K. Watanabe, T. Taniguchi, A. C. Ferrari, and M. Atatüre, Atomically thin quantum light-emitting diodes, *Nature Communications* **7**, 1 (2016), 1603.08795.
 - [18] L. A. Jauregui, A. Y. Joe, K. Pistunova, D. S. Wild, A. A. High, Y. Zhou, G. Scuri, K. de Greve, A. Sushko, C. H. Yu, T. Taniguchi, K. Watanabe, D. J. Needleman, M. D. Lukin, H. Park, and P. Kim, Electrical control of interlayer exciton dynamics in atomically thin heterostructures, *Science* **366**, 870 (2019).
 - [19] R. S. Sundaram, M. Engel, A. Lombardo, R. Krupke, A. C. Ferrari, P. Avouris, and M. Steiner, Electroluminescence in single layer mos₂, *Nano Letters* **13**, 1416 (2013).
 - [20] J. S. Ross, P. Klement, A. M. Jones, N. J. Ghimire, J. Yan, D. G. Mandrus, T. Taniguchi, K. Watanabe, K. Kitamura, W. Yao, D. H. Cobden, and X. Xu, Electrically tunable excitonic light-emitting diodes based on monolayer WSe₂ p-n junctions, *Nature Nanotechnology* **9**, 268 (2014).
 - [21] S. Z. Uddin, N. Higashitarumizu, H. Kim, I. K. M. R. Rahman, and A. Javey, Efficiency Roll-Off Free Electroluminescence from Monolayer WSe₂, *Nano Letters* **10.1021/acs.nanolett.2c01311** (2022).
 - [22] F. Withers, O. Del Pozo-Zamudio, S. Schwarz, S. Dufferwiel, P. M. Walker, T. Godde, A. P. Rooney, A. Gholinia, C. R. Woods, P. Blake, S. J. Haigh, K. Watanabe, T. Taniguchi, I. L. Aleiner, A. K. Geim, V. I. Fal'ko, A. I. Tartakovskii, and K. S. Novoselov, WSe₂ Light-Emitting Tunneling Transistors with Enhanced Brightness at Room Temperature, *Nano Letters* **15**, 8223 (2015).
 - [23] Q. Fu, Z. Hu, M. Zhou, J. Lu, and Z. Ni, Excitonic Emission in Atomically Thin Electroluminescent Devices, *Laser and Photonics Reviews* **2000587**, 1 (2021).
 - [24] J. Binder, J. Howarth, F. Withers, M. R. Molas, T. Taniguchi, K. Watanabe, C. Faugeras, A. Wysmolek, M. Danovich, V. I. Fal'ko, A. K. Geim, K. S. Novoselov, M. Potemski, and A. Kozikov, Upconverted electroluminescence via Auger scattering of interlayer excitons in van der Waals heterostructures, *Nature Communications* **10**, 1 (2019), 1905.10076.
 - [25] G. Clark, J. R. Schaibley, J. Ross, T. Taniguchi, K. Watanabe, J. R. Hendrickson, S. Mou, W. Yao, and X. Xu, Single defect light-emitting diode in a van der waals heterostructure, *Nano letters* **16**, 3944 (2016).
 - [26] L. E. P. López, A. Rosławska, F. Scheurer, S. Berciaud, and G. Schull, Tip-induced excitonic luminescence nanoscopy of an atomically-resolved van der Waals heterostructure, , 1 (2022), arXiv:2204.14022.
 - [27] R. J. P. Román, D. Pommier, R. Bretel, L. E. P. López, E. Lorchat, J. Chaste, A. Ouerghi, S. L. Moal, E. Boer-Duchemin, G. Dujardin, A. G. Borisov, L. F. Zagonel, G. Schull, S. Berciaud, and E. L. Moal, Electroluminescence of monolayer WS₂ in a scanning tunneling microscope: the effect of bias polarity on the spectral and angular distribution of the emitted light, (2022), arXiv:2205.12789.
 - [28] J. Feng, Y. Li, J. Zhang, Y. Tang, H. Sun, L. Gan, and C. Z. Ning, Injection-free multiwavelength electroluminescence devices based on monolayer semiconductors driven by an alternating field, *Science Advances* **8**, 1 (2022).
 - [29] T. Förster, *Delocalized Excitation and Excitation Transfer. Bulletin No. 18*, Tech. Rep. (Florida State Univ., Tallahassee. Dept. of Chemistry, 1964).
 - [30] L. Novotny and B. Hecht, *Principles of nano-optics* (Cambridge university press, 2012).
 - [31] S. Weiss, Fluorescence spectroscopy of single biomolecules, *Science* **283**, 1676 (1999).
 - [32] R. E. Dale and J. Eisinger, Intramolecular energy transfer and molecular conformation, *Proceedings of the National Academy of Sciences of the United States of America* **73**, 271 (1976).
 - [33] C. R. Kagan, C. B. Murray, M. Nirmal, and M. G. Bawendi, Electronic energy transfer in CdSe Quantum dot solids, *Physical Review Letters* **76**, 1517 (1996).
 - [34] H. Van Amerongen, R. Van Grondelle, *et al.*, *Photosynthetic excitons* (World Scientific, 2000).
 - [35] M. Achermann, M. A. Petruska, D. D. Koleske, M. H. Crawford, and V. I. Klimov, Nanocrystal-based light-emitting diodes utilizing high-efficiency nonradiative energy transfer for color conversion, *Nano Letters* **6**, 1396 (2006).
 - [36] S. Pimputkar, J. S. Speck, S. P. Denbaars, and S. Nakamura, Prospects for LED lighting, *Nature Photonics* **3**, 180 (2009).
 - [37] M. Parzefall, P. Bharadwaj, A. Jain, T. Taniguchi, K. Watanabe, and L. Novotny, Antenna-coupled photon emission from hexagonal boron nitride tunnel junctions, *Nature nanotechnology* **10**, 1058 (2015).
 - [38] M. Parzefall, Á. Szabó, T. Taniguchi, K. Watanabe, M. Luisier, and L. Novotny, Light from van der waals quantum tunneling devices, *Nature communications* **10**, 1 (2019).
 - [39] E. Lorchat, L. E. P. López, C. Robert, D. Lagarde, G. Froehlicher, T. Taniguchi, K. Watanabe, X. Marie, and S. Berciaud, Filtering the photoluminescence spectra of atomically thin semiconductors with graphene, *Nature Nanotechnology* **15**, 283 (2020).
 - [40] J. A. Schuller, S. Karav eli, T. Schiros, K. He, S. Yang, I. Kyymissis, J. Shan, and R. Zia, Orientation of luminescent excitons in layered nanomaterials, *Nature nanotechnology* **8**, 271

- (2013).
- [41] G. Ford and W. Weber, Electromagnetic interactions of molecules with metal surfaces, *Physics Reports* **113**, 195 (1984).
 - [42] D. L. Andrews and D. S. Bradshaw, Virtual photons, dipole fields and energy transfer: a quantum electrodynamical approach, *European Journal of Physics* **25**, 845 (2004).
 - [43] M. Parzefall, P. Bharadwaj, and L. Novotny, Antenna-coupled tunnel junctions, in *Quantum plasmonics* (Springer, 2017) pp. 211–236.
 - [44] A. Karmakar, A. Al-Mahboob, C. E. Petoukhoff, O. Kravchyna, N. S. Chan, T. Taniguchi, K. Watanabe, and K. M. Dani, Dominating Interlayer Resonant Energy Transfer in Type-II 2D Heterostructure, *ACS Nano* **16**, 3861 (2022).
 - [45] F. Prins, A. J. Goodman, and W. A. Tisdale, Reduced dielectric screening and enhanced energy transfer in single- and few-layer mos₂, *Nano Letters* **14**, 6087 (2014).
 - [46] Y. Ye, Z. J. Wong, X. Lu, X. Ni, H. Zhu, X. Chen, Y. Wang, and X. Zhang, Monolayer excitonic laser, *Nature Photonics* **9**, 733 (2015), 1503.06141.
 - [47] E. Y. Paik, L. Zhang, G. W. Burg, R. Gogna, E. Tutuc, and H. Deng, Interlayer exciton laser of extended spatial coherence in atomically thin heterostructures, *Nature* **576**, 80 (2019), 1901.00598.
 - [48] S. H. Oh, H. Altug, X. Jin, T. Low, S. J. Koester, A. P. Ivanov, J. B. Edel, P. Avouris, and M. S. Strano, Nanophotonic biosensors harnessing van der Waals materials, *Nature Communications* **12**, 1 (2021).

Supplementary materials for Energy transfer from tunneling electrons to excitons

Sotirios Papadopoulos,^{1,*} Lujun Wang,^{1,*} Takashi Taniguchi,² Kenji Watanabe,³ and Lukas Novotny^{1,†}

¹Photonics Laboratory, ETH Zurich, 8093 Zurich, Switzerland.

²International Center for Materials Nanoarchitectonics,

National Institute for Materials Science, 1-1 Namiki, Tsukuba 305-0044, Japan

³Research Center for Functional Materials, National Institute for Materials Science, 1-1 Namiki, Tsukuba 305-0044, Japan

Materials and methods

Sample fabrication MoSe₂, WSe₂, graphene and hBN flakes are mechanically exfoliated from bulk crystals on Si/SiO₂ substrates with the scotch tape method. The hBN flakes are exfoliated in air the other flakes in argon (Ar) atmosphere. The Si/SiO₂ substrates are first cleaned in an oxygen plasma asher for 5 minutes. The heterostructures are fabricated by a dry pick-up and transfer technique [1] as follows: A poly-dimethylsiloxane (PDMS) stamp, covered by a thin polycarbonate (PC) film, is used to sequentially pick-up all flakes from their substrate at 80 °C in Ar atmosphere in a glovebox. The resulting stack is then transferred on top of pre-patterned gold electrodes on a glass substrate by heating up the substrate to 170 °C in order to melt the PC film and allow it to detach from the PDMS stamp. In that way, the stack is transferred on top of the gold electrodes. Later, the PC film is dissolved in a chloroform bath for 30 minutes. The gold electrodes are pre-patterned by photolithography followed by e-beam evaporation of 5 nm Ti (adhesion layer) and 50 nm gold. Metal lift-off is done in an acetone bath at 60 °C.

Electrical and optical characterization The gold electrodes on the sample's substrate are wire-bonded to adhesive copper pads that allow conductive contact to co-axial connections to a Keithley Source Meter 2602B, that is used as a voltage source and current meter. The sample is then put, facing down, on a Nikon TE300 inverted microscope in ambient conditions. The light emitted by the device under bias voltage is collected by a 100x objective with 0.9 NA. All spectra are measured by imaging the real space of emission at the entrance of a Princeton Instruments Acton SpectraPro 300i spectrometer. The real and Fourier space (back-focal plane) of emission is imaged at the entrance of an Andor iXon Ultra camera. Finally, all PL measurements were collected by optically exciting the sample with a 532 nm solid state laser.

Density of optical states The dissipated power P of a point electric dipole is calculated by [2]

$$P = \frac{1}{2} \omega \mathbf{p} \cdot \text{Im}\{\mathbf{E}(\mathbf{r}_0)\} \quad (1)$$

where ω is the angular frequency of the dipole's emission, \mathbf{p} is the dipole moment and \mathbf{E} is the electric field at the dipoles origin \mathbf{r}_0 . The dipole is assumed to be situated at the center of the tunneling hBN layer. The electric field $\mathbf{E}(\mathbf{r}_0)$ is calculated by solving the electromagnetic wave equation for a multi-layer structure. The optical density of states ρ_{opt} is then calculated through its relation to P [2]

$$\frac{\rho_{\text{opt}}}{\rho_0} = \frac{P}{P_0} \quad (2)$$

with P_0 being the dissipated power for a point dipole in vacuum.

Exciton to photon coupling ratio We calculate the ratio $\eta_{e-x}/\eta_{e-\gamma}$ using the following relationship,

$$\frac{I_x}{I_\gamma} = \frac{\eta_{e-x} \cdot \eta_{x-\gamma} \cdot \eta_{col}^{\rightarrow}}{\eta_{e-\gamma} \cdot \eta_{col}^{\uparrow}} \quad (3)$$

where I_x is the exciton coupled emission, I_γ is the photon coupled emission, η_{col}^{\rightarrow} and η_{col}^{\uparrow} is the collection efficiency for an in-plane and an out-of-plane dipole, respectively. The $\eta_{x-\gamma}$ expresses the PL efficiency of the WSe₂ flake which is measured to be around $1.5 \cdot 10^{-5}$. The low value results from graphene quenching [3].

Exciton generation rate The exciton generation rate calculated in Eq. 1 in the main text involves the inelastic tunneling rate spectrum γ_{inel} which is a function of the electronic density of states of the right and left electrodes (ρ_R and ρ_L , respectively), the optical density of states ρ_{opt} and the applied V_b . It is calculated by [4, 5],

$$\gamma_{inel}(\hbar\omega) = \frac{\rho_{opt}(\hbar\omega)\pi e^2}{3\hbar\omega m^2 \epsilon_0} \int_{\hbar\omega}^{eV_b} |\mathcal{P}(E, \hbar\omega)|^2 \rho_R(E - \hbar\omega) \rho_L(E) dE \quad (4)$$

where \mathcal{P} is the momentum matrix element, m is the electrons mass, ϵ_0 is the vacuum permittivity and e is the elementary charge.

Emission comparison between different devices To be able to compare the rate of excitonic emission of different devices we normalize the measured emission intensity I_x by the area of emission and by the relative PL efficiency of the flake. Finally we normalize by the photon-coupled background emission I_γ in every device. This normalization is necessary because in every device the tunneling barrier thickness may vary by ± 0.33 nm. This has a minor effect on the optical coupling but it can drastically affect γ_{inel} through the momentum matrix element \mathcal{P} (Eq. 4). This impacts the exciton generation rate Γ_x making the direct comparison between different devices impossible. Since I_γ is directly proportional to \mathcal{P} we use it to normalize the I_x emission and be able to compare devices with different TMD to tunnel junction distance (Fig. 4 in the main text).

Conductance measurements

We electrically characterize the device by applying a bias voltage (V_b) between the gold and graphene electrodes as indicated in Fig. S1A. The current and conductance measurements are shown in Fig. S1B. The triple minima in the conductance curve around 0 V are associated with the intrinsic graphene doping and the phonon induced tunneling that governs the transport of such devices, as it has been investigated in previous studies [6–8]. This indicates that tunneling indeed occurs between graphene and gold and is phonon-mediated. Moreover, for $V_b < 1.5$ V the conductance shows a linear behavior. In this low voltage regime compared to the hBN barrier (5 eV) the conductance curve is associated to the linear density of states of graphene. Interestingly, around $V_b = 1.5$ V and -1.7 V, the slope of the conductance increases. This behavior is not observed in devices without a WSe₂ and can be associated with an increased rate due to interaction of the tunneling electrons with excitonic states.

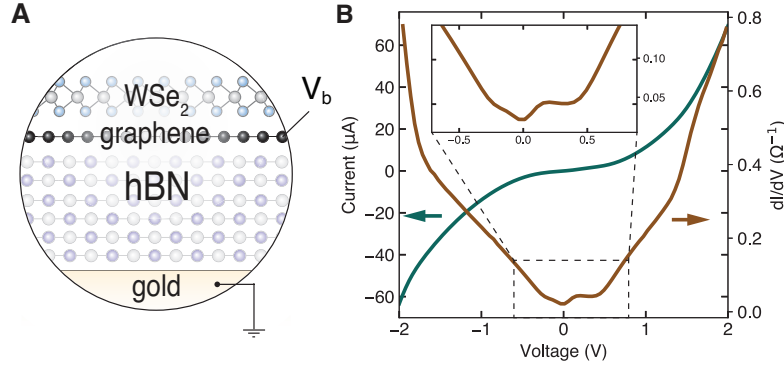


FIG. S1. **Electrical characterization.** Device schematic of a TMD coupled tunneling junction. Current and conductance (dI/dV) measurements as a function of V_b .

Exciton generation in both polarities

As discussed in the main text the exciton generation process occurs for both bias polarities. Figure S2 shows spectra for both polarities where the narrow emission at exciton wavelengths is observed. This indicates excitons are not generated by electron-hole injection since such a process, if possible, would be strictly polarity dependent.

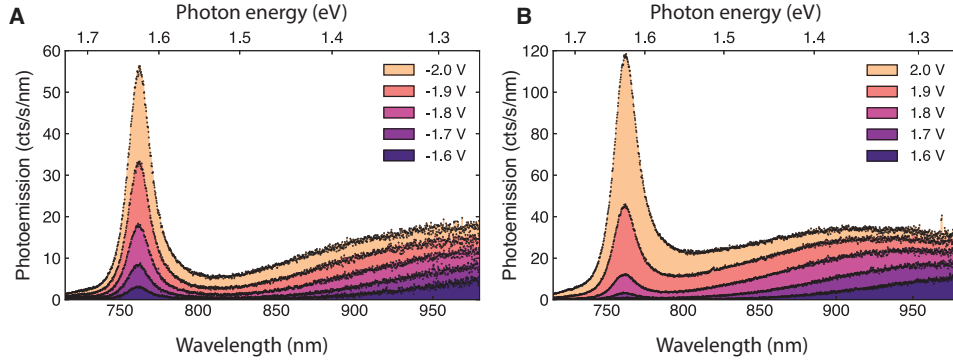


FIG. S2. **Spectral symmetry with bias voltage.** (a,b) Photoemission spectra from the TMDC coupled tunneling junction presented in Fig. 2A in the main text for (a) positive bias voltage and (b) negative bias voltage. Similar spectral characteristics are observed. This observation further supports the argument that there excitons are not created by charge injection as such a process would be polarity dependent.

TMD coupled device with 5 nm spacer hBN

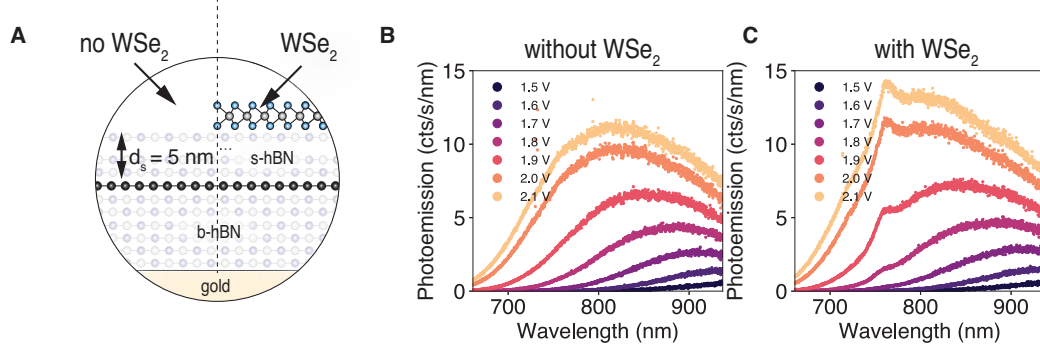


FIG. S3. **TMD coupled device with 5 nm spacer hBN.** (a) Device schematic. The WSe₂ is separated from the tunneling junction by a spacer hBN with 5 nm thickness. The WSe₂ flake is stacked on top in a way that two areas are formed: with and without WSe₂. (b,c) Photoemission spectra from the two areas (b) without WSe₂ and (c) with WSe₂. A small contribution in excitonic wavelengths is still observed even though the WSe₂ flake is 5 nm away from the tunneling junction.

* These two authors contributed equally

† inovotny@ethz.ch

- [1] P. Zomer, M. Guimarães, J. Brant, N. Tombros, and B. Van Wees, Fast pick up technique for high quality heterostructures of bilayer graphene and hexagonal boron nitride, *Applied Physics Letters* **105**, 013101 (2014).
- [2] L. Novotny and B. Hecht, *Principles of nano-optics* (Cambridge university press, 2012).
- [3] E. Lorchat, L. E. P. López, C. Robert, D. Lagarde, G. Froehlicher, T. Taniguchi, K. Watanabe, X. Marie, and S. Berciaud, Filtering the photoluminescence spectra of atomically thin semiconductors with graphene, *Nature Nanotechnology* **15**, 283 (2020).
- [4] M. Parzefall and L. Novotny, Optical antennas driven by quantum tunneling: a key issues review, *Reports on Progress in Physics* **82**, 112401 (2019).
- [5] M. Parzefall, P. Bharadwaj, and L. Novotny, Antenna-coupled tunnel junctions, in *Quantum plasmonics* (Springer, 2017) pp. 211–236.
- [6] Y. Zhang, V. W. Brar, F. Wang, C. Girit, Y. Yayan, M. Panlasigui, A. Zettl, and M. F. Crommie, Giant phonon-induced conductance in scanning tunnelling spectroscopy of gate-tunable graphene, *Nature Physics* **4**, 627 (2008).
- [7] E. E. Vdovin, A. Mishchenko, M. Greenaway, M. Zhu, D. Ghazaryan, A. Misra, Y. Cao, S. Morozov, O. Makarovskiy, T. Fromhold, *et al.*, Phonon-assisted resonant tunneling of electrons in graphene–boron nitride transistors, *Physical review letters* **116**, 186603 (2016).
- [8] M. Parzefall, Á. Szabó, T. Taniguchi, K. Watanabe, M. Luisier, and L. Novotny, Light from van der waals quantum tunneling devices, *Nature communications* **10**, 1 (2019).